analytical chemistry

pubs.acs.org/ac Article

Toehold-Mediated Cascade Catalytic Assembly for Mycotoxin Detection and Its Logic Applications

Jiafeng Pan, Fang Deng, Zhi Liu, Gu Shi, and Junhua Chen*

Cite This: *Anal. Chem.* 2022, 94, 3693−3700 Read Online

ACCESS | Metrics & More | Article Recommendations | Supporting Information

ABSTRACT: In this work, an enzyme-free biosensor is reported for mycotoxin detection based on a toehold-mediated catalytic hairpin assembly (CHA) and a DNAzyme-cascaded hydrolysis reaction. In the presence of a mycotoxin, the recognition between an aptamer and the mycotoxin releases the trigger DNA. The trigger DNA initiates the toehold-mediated CHA, generating large amounts of partial duplex B/C with four toeholds, which can be used to assemble the DNAzyme-cascaded hydrolysis reaction. Furthermore, through a collaborative autoassembly reaction among the B/C duplex, DNA1, and DNA2, supramolecular nanostructures corresponding to Mg^{2+}-dependent DNAzymes can be formed. With the incubation of Mg^{2+}, the dual-modified (TAMRA/BHQ2) substrate strand DNA2 will be cleaved into two fragments, yielding a high TAMRA fluorescence signal for mycotoxin testing. Under optimal conditions, the sensing system was ultrasensitive and showed low detection limits of 0.2 pM for ochratoxin A (OTA), 0.13 pM for aflatoxin B1 (AFB1), and 0.17 pM for zearalenone (ZEN). The mycotoxin aptasensor also exhibited high selectivity and was successfully applied for the quantitative analysis of OTA, AFB1, and ZEN in wine samples. Due to the advantages of flexibility and versatility, this mycotoxin platform was used to fabricate several concatenated logic gates including "AND−INHIBIT", "INHIBIT−OR", "OR−AND", and "OR−INHIBIT" logic biocomputings. Such multiple functions of the logic system provided a universal sensing strategy for the intelligent detection of multiplex mycotoxins, demonstrating considerable potential in food safety and environmental monitoring.

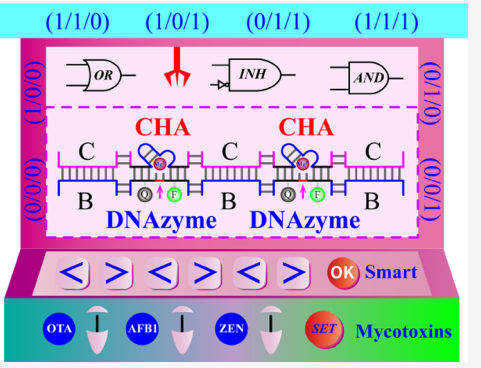

Mycotoxins are the poisonous secondary metabolites generated by fungi, which contaminate various foods, including dried fruits, cereals, and wine.[1,2] Extensive studies have reported that many mycotoxins are carcinogenic, hepatotoxic, nephrotoxic, and immunotoxic agents causing side effects to human beings.[3] Considering their potential toxic effects, maximum acceptable concentrations have been established for several mycotoxins in cereals, such as 5 μg/kg for ochratoxin A (OTA), 2 μg/kg for aflatoxin B1 (AFB1), and 100 μg/kg for zearalenone (ZEN).[4] Currently, some conventional analytical methods have been developed for mycotoxin monitoring, such as high-performance liquid chromatography (HPLC),[5] gas chromatography−tandem mass spectrometry (GC-MS/MS),[6] and high-performance liquid chromatography−tandem mass spectrometry (HPLC-MS/MS).[7] Alternatively, several aptasensors have been successfully designed for mycotoxin assays using colorimetric,[8−10] fluorescence,[11] electrochemical,[12−14] and surface-enhanced Raman scattering sensing platforms.[15,16] However, intelligent detection of multiplex mycotoxins is still a challenge.

Molecular computations have attracted significant research interest, resulting in the remarkable progress of Boolean logic systems, such as AND, NAND, XOR, and INHIBIT.[17−23] DNA logic gates often utilize colorimetric,[24−26] fluorescence,[27−32] or electrochemical signals as reporting outputs,[33−36] which perform arithmetic calculations or even play "tic-tac-toe". With the increasing demands for disease diagnostics, biochemical sensing, and biomedical imaging,[37] advanced computing gates have been developed including keypad lock,[38−41] half-adder/subtractor,[42,43] and multiplexer.[44,45] However, most of the molecular computations suffer from low sensitivity, imposing restrictions on practical applications. To improve the detection sensitivity, a toehold-mediated cascade catalytic assembly can serve as an ideal tool for signal amplification.

To explore new strategies for mycotoxin detection, we report an enzyme-free toehold-mediated cascade catalytic assembly for a mycotoxin assay. Based on the toehold-mediated cascade catalytic hairpin assembly (CHA) and a DNAzyme-cascaded hydrolysis reaction, the constructed mycotoxin aptasensor showed high sensitivity, excellent selectivity, and good reproducibility toward OTA, AFB1, and

Received: December 19, 2021
Accepted: February 8, 2022
Published: February 18, 2022

https://doi.org/10.1021/acs.analchem.1c05485
Anal. Chem. 2022, 94, 3693−3700

ZEN, respectively. In addition, we explored the logic biocomputings of the proposed platform, and four different logic functions of "AND−INHIBIT, INHIBIT−OR, OR−AND, and OR−INHIBIT" were constructed.

EXPERIMENTAL SECTION

Chemicals and Materials. Mycotoxin standard substances including OTA, AFB1, ZEN, ochratoxin B (OTB), aflatoxin M1 (AFM1), deoxynivalenol (DON), aflatoxin G1 (AFG1), altenuene (ALT), aflatoxin G2 (AFG2), fumonisin (FB1), and aflatoxin B2 (AFB2) were bought from Sigma-Aldrich (Shanghai, China). White wine was obtained from the local supermarket (Guangzhou, China). All other chemicals were analytical grade and obtained from Beijing Solarbio Science and Technology Co., Ltd. (Beijing, China). The HPLC-purified DNA sequences were offered by Sangon Biotech Co., Ltd. (Shanghai, China) and are listed in Tables S1−S5 (Supporting Information). Ultrapure water (18.2 MΩ/cm) was used in the whole experiment.

Analytical Procedure. All DNA probes were dissolved in 10 mM Tris−HCl buffer (pH 8.0, 120 mM NaCl, 10 mM $MgCl_2$, 5 mM KCl, 20 mM $CaCl_2$). All hairpins (A, B, and C) were heated to 97 °C for 5 min and allowed to cool down to room temperature. For OTA detection, 250 nM probe A, 250 nM probe B, 500 nM probe C, 250 nM enzyme strand DNA1, and 250 nM substrate strand DNA2 were incubated with different concentrations of OTA at 25 °C for 90 min. The fluorescence spectra were recorded from 570 to 700 nm (E_x = 545 nm, E_m = 585 nm). The fluorescence signals were recorded using a SpectraMax i3x (Molecular Devices). For AFB1 and ZEN detection, different concentrations of AFB1 and ZEN were mixed with 250 nM probes S and Z, respectively. Other procedures were the same as that for OTA detection.

Specificity. To evaluate the specificity, a panel of toehold-mediated cascade catalytic assemblies were successively tested toward different mycotoxins including OTA, AFB1, ZEN, OTB, AFM1, DON, AFG1, ALT, AFG2, FB1, and AFB2.

Wine Sample Analysis. Different concentrations of OTA, AFB1, and ZEN were simultaneously spiked into the wine samples and detected directly without any pretreatments except for dilution with a buffer solution. The spiked samples were further quantified using our mycotoxin biosensor and the liquid chromatography−mass spectrometry (LC-MS/MS) method.

Polyacrylamide Gel Electrophoresis (PAGE). A 10% PAGE gel was prepared for electrophoresis analysis, in which 1.0 mL of 10× Tris/borate/ethylenediaminetetraacetic acid (EDTA) (TBE) buffer, 3.3 mL of 30% acrylamide/bisacrylamide gel solution (29:1), 5.5 mL of ultrapure water, 100 μL of ammonium persulfate (10%), and 10 μL of *N,N,N′,N′*-tetramethylethylenediamine were mixed and polymerized at room temperature for 3.5 h. Then, the loading samples were mixed with 4 μL of the resulting solution, 1 μL of 6× loading buffer, and 1 μL of 100× SYBR Green solution. Subsequently, the electrophoresis experiments were carried out at 60 V for 90 min in 1× TBE buffer (89 mM Tris base, 89 mM boric acid, 2 mM EDTA, pH = 8.0). Finally, the PAGE gel was scanned using a gel image analysis system (Bio-Rad, Singapore).

Logic Gate Operations. In the connected logic gate operations, 10 nM OTA, 10 nM AFB1, and 10 nM ZEN were used as three inputs to activate the sensing platform. Hairpin probes D, E, and F were used as sensing elements in the "AND−INHIBIT" connected logic gate. In the "INHIBIT−OR" connected logic gate, hairpin probes A, G, and S were used as sensing elements. Hairpin probes D, H, and I were used as sensing elements in the "OR−AND" connected logic gate. Hairpin probes A, S, and J were used as sensing elements in the "OR−INHIBIT" connected logic gate. Other procedures were the same as that for OTA detection in the sensing system.

RESULTS AND DISCUSSION

The working principle of the toehold-mediated cascade catalytic assembly for mycotoxin detection is shown in Scheme 1. Three hairpin probes (A, B, and C), enzyme strand DNA1, and substrate strand DNA2 were used in the sensing system. OTA was used as the model target. Probe A contains the OTA aptamer (blue part) and the trigger DNA (domains a and b, red part). When OTA is introduced into the sensing system, the specific binding between the aptamer and OTA leads to the release of the complementary trigger DNA, which can act as an initiator sequence to launch the toehold-mediated cascade catalytic assembly. The trigger DNA first hybridizes with the toehold (domain a*) of probe B to initiate CHA. The hybridization between the trigger DNA and probe B opens probe B, thus facilitating the formation of the OTA/A/B complex *via* toehold binding and branch migration. Then, the newly exposed sticky end (domain b) of unfolded probe B can bind to the toehold (domain b*) of probe C and form the intermediate OTA/A/B/C. This intermediate will give rise to a branch migration process to liberate the OTA/A complex, further generating partial duplex B/C with four toeholds. In

Scheme 1. Schematic Illustration of the Detection Mechanism Based on a Toehold-Mediated Cascade Catalytic Assembly and Supramolecular DNAzyme Nanostructures ($[B/C/DNA1/DNA2]_n$) for Mycotoxin Detection

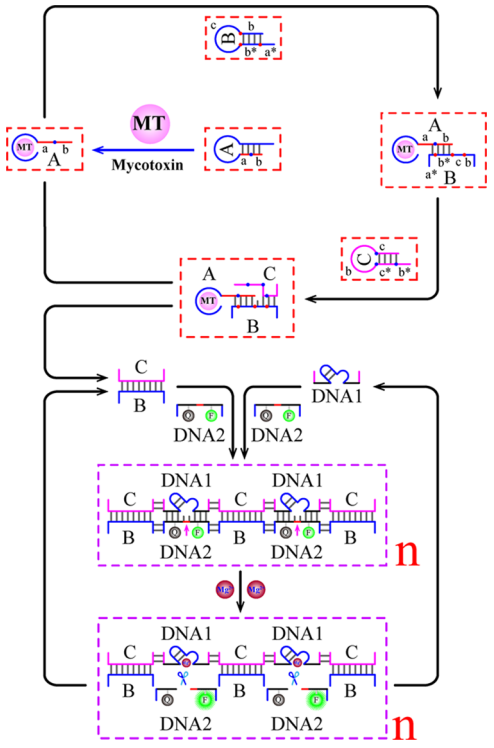

https://doi.org/10.1021/acs.analchem.1c05485
Anal. Chem. 2022, 94, 3693−3700

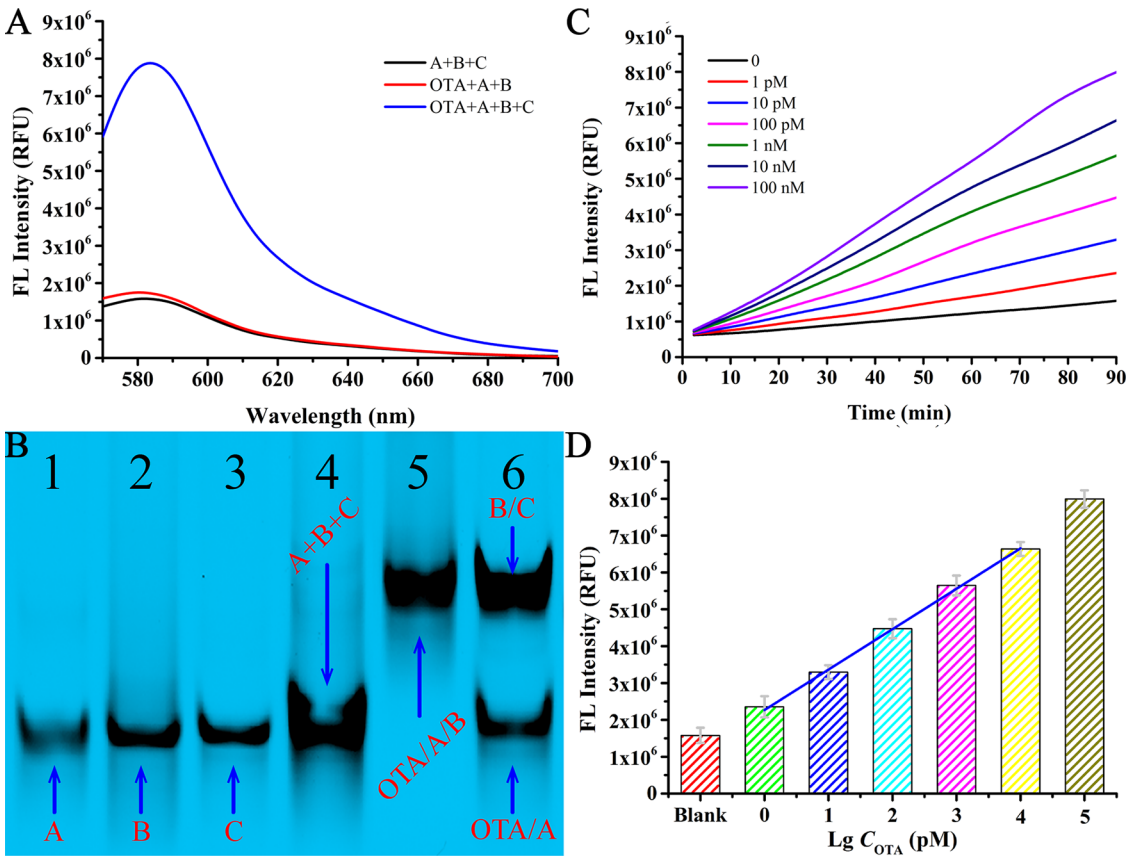

Figure 1. (A) Fluorescence spectra of the assay solution under different controls, including A + B + C, OTA + A + B, and OTA + A + B + C. (B) Polyacrylamide gel electrophoresis analysis of the assembly process. Lane 1, A; lane 2, B; lane 3, C; lane 4, A + B + C; lane 5, OTA + A + B; and lane 6, OTA + A + B + C. (C) Time-dependent fluorescence signals of the DNAzyme-cascaded hydrolysis reaction in the presence of different OTA concentrations. (D) Fluorescence responses of the toehold-mediated cascade catalytic assembly toward OTA at different concentrations. Reaction time, 90 min.

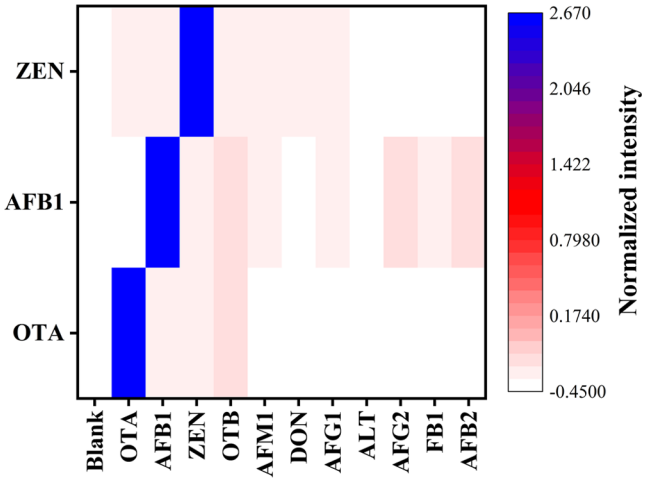

Figure 2. Heat map results of the orthogonal experiments for mycotoxin detection. The concentration of each mycotoxin is 10 nM.

this way, the recycling of the OTA/A complex is realized to amplify the response signal, and large amounts of B/C can be produced, which can be used to assemble a DNAzyme-cascaded hydrolysis reaction. Through a collaborative autoassembly reaction among the B/C duplex, DNA1, and DNA2, supramolecular nanostructures ($[B/C/DNA1/DNA2]_n$) corresponding to Mg^{2+}-dependent DNAzymes can be formed. In the presence of Mg^{2+}, the dual-modified (TAMRA/BHQ2) substrate strand DNA2 will be cleaved into two fragments, resulting in the spontaneous dissociation of DNA1 from the B/C duplex. The free B/C duplex and DNA1 can trigger other DNAzyme-cascaded hydrolysis reactions. The separation of the fluorophore and quencher yields a high TAMRA fluorescence signal for OTA testing. In the absence of OTA, all hairpin probes are stable and the toehold-mediated cascade catalytic assembly cannot be triggered. As a result, only a background fluorescence signal can be obtained.

To evaluate the feasibility of the toehold-mediated cascade catalytic assembly for mycotoxin detection, the fluorescence signals of the sensing system were recorded under different controls using OTA as the model target. As shown in Figure 1A, only a weak background signal can be observed in the absence of OTA (black line). This suggested that without OTA, the toehold-mediated cascade catalytic assembly is inhibited and DNA2 cannot be cleaved. In the presence of OTA but without probe C in the sensing system, no obvious fluorescence response can be obtained (red line), indicating that the signal amplifications of the CHA and DNAzyme-cascaded hydrolysis reaction cannot happen and no DNA2 is cleaved. Significantly, when probe C is added into this system, the response signal is sharply increased (blue line). The reason is that the toehold-mediated cascade catalytic assembly can be completed, leading to the cleavage of DNA2 for signal output. Meanwhile, the reaction process of the toehold-mediated CHA

https://doi.org/10.1021/acs.analchem.1c05485
Anal. Chem. 2022, 94, 3693−3700

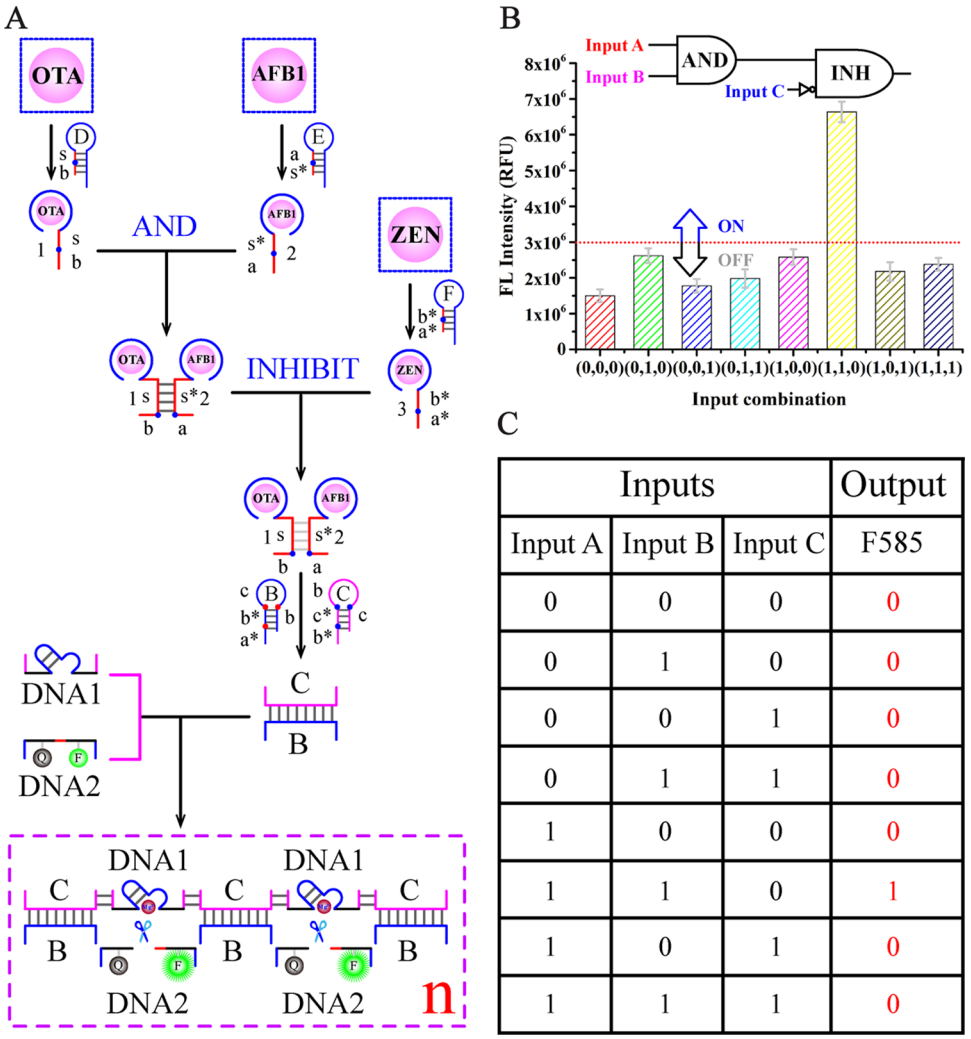

C

Inputs			Output
Input A	Input B	Input C	F585
0	0	0	0
0	1	0	0
0	0	1	0
0	1	1	0
1	0	0	0
1	1	0	1
1	0	1	0
1	1	1	0

Figure 3. (A) Schematic illustration of the AND−INHIBIT logic gate. (B) Histogram presentation of the corresponding fluorescence intensities at 585 nm. The red dashed line shows the threshold value of 3.0 × 10^6. (C) Truth table of the AND−INHIBIT logic gate.

was further confirmed by PAGE images (Figure 1B). In addition, the formation of supramolecular nanostructures ($[B/C/DNA1/DNA2]_n$) corresponding to Mg^{2+}-dependent DNAzymes was also verified by PAGE results (Figure S1, Supporting Information). These results evidenced that the toehold-mediated cascade catalytic assembly can feasibly provide an amplified fluorescence signal for mycotoxin detection.

Under optimized assay conditions (Figures S2−S5, Supporting Information), the constructed biosensor was first used for OTA detection at different concentrations. As depicted in Figure 1C, the response signals increased gradually with increasing OTA concentrations from 0 to 100 nM. The linear relationship between the fluorescence signal and the logarithm of OTA concentration was achieved in the range from 1 pM to 10 nM (R^2 = 0.995) with a detection limit of 0.2 pM (3S/N, Figure 1D). Furthermore, by replacing the OTA aptamer sequence with an AFB1 or ZEN aptamer sequence, the sensing system can be used to detect AFB1 or ZEN. The analytical performance of the biosensor for AFB1 detection is shown in Figure S6 (Supporting Information). There was a linear correlation between the fluorescence signal and the logarithmic value of AFB1 concentration ranging from 1 pM to 10 nM (R^2 = 0.994), and the detection limit of AFB1 was calculated to be 0.13 pM (3S/N). As shown in Figure S7 (Supporting Information), a similar linear relationship between the fluorescence signal and the logarithmic value of ZEN was observed with a detection limit of 0.17 pM (3S/N). The sensitivity of our proposed method is comparable or even superior to those of some previously reported biosensors for mycotoxin detection (Table S6, Supporting Information).

To assess the specificity, a panel of toehold-mediated cascade catalytic assemblies were tested toward different mycotoxins (OTA, AFB1, ZEN, OTB, AFM1, DON, AFG1, ALT, AFG2, FB1, and AFB2). The detection results are shown as a heat map in Figure 2. Each sensing system selectively responded to its target mycotoxin with a low cross-response, indicating that the toehold-mediated cascade catalytic assembly had a high specificity toward OTA, AFB1, or ZEN, which could be attributed to the high affinity between the aptamer and mycotoxin.

To investigate the practical detection performance for mycotoxins in white wine, a recovery experiment was performed. Wine samples were spiked with different concentrations of mycotoxins. As listed in Table S7 (Supporting Information), the recoveries were in the range of 96−105.7% with relative standard deviations of 4.7−7.3%. The concentration of mycotoxin in the spiked wine samples

https://doi.org/10.1021/acs.analchem.1c05485
Anal. Chem. 2022, 94, 3693−3700

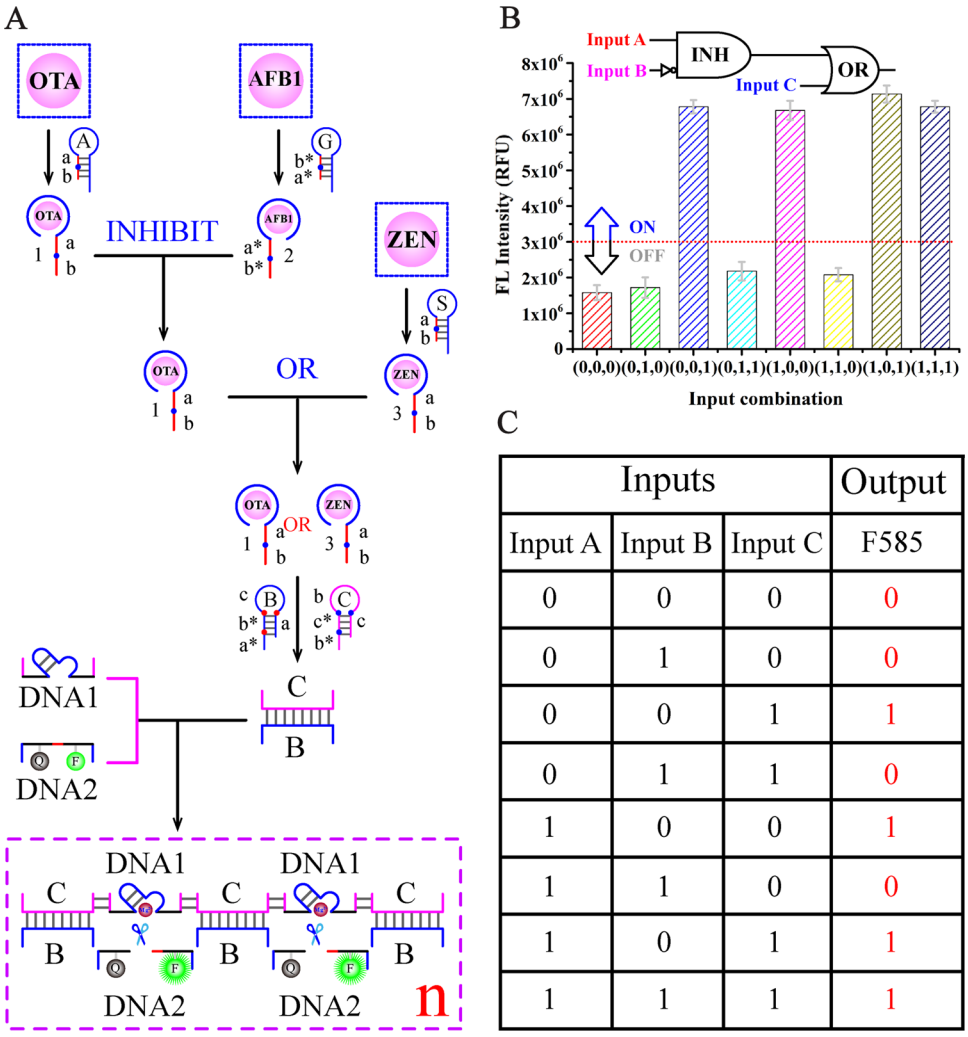

C

Inputs			Output
Input A	Input B	Input C	F585
0	0	0	0
0	1	0	0
0	0	1	1
0	1	1	0
1	0	0	1
1	1	0	0
1	0	1	1
1	1	1	1

Figure 4. (A) Schematic illustration of the INHIBIT−OR logic gate. (B) Histogram presentation of the corresponding fluorescence intensities at 585 nm. The red dashed line shows the INHIBIT−OR logic gate. (C) Truth table of the INHIBIT−OR logic gate.

was further confirmed by the LC-MS/MS method. The data revealed that no significant difference existed between the values measured using our proposed biosensor and the LC-MS/MS method. The relative error (Re) was in the range of −2.4 to 6.6%. The results confirmed the practical applicability of the developed method for the reliable detection of OTA, AFB1, and ZEN in real samples.

Considering the coexistence of various mycotoxins in food, three-input concatenated logic circuits were constructed. OTA, AFB1, and ZEN were set as input A, input B, and input C, respectively. The inputs were coded as "1" when they were present and "0" when they were absent. The fluorescence intensities below and above the threshold value of 3×10^6 were set as 0 and 1, respectively. Inputs of concentration 10 nM were used in the logic operations. Such an input concentration is superior to those used in some previously reported logic gates (Table S8, Supporting Information). First, we proposed an AND−INHIBIT connected logic gate (Figure 3A). In the presence of input A, the hairpin probe D will bind to OTA and release the trigger DNA 1 (domains s and b). Similarly, the trigger DNA 2 (domains a and s*) will also be released in the presence of input B. Then, domain s in probe D will hybridize with domain s* in probe E to form a partial duplex complex (1−2). In the same way, with the addition of input C, the recognition binding between probe F and ZEN will lead to the release of the trigger DNA 3 (domains b* and a*). The complex (1−2) and the trigger DNA 3 (domains b* and a*) are complementary nucleic acids. If the trigger DNA 3 (domains b* and a*) is liberated in the logic system, it will prevent the complex (1−2) from launching the toehold-mediated cascade catalytic assembly. Thus, the complex (1−2) containing unpaired domains (b and a) can hybridize with the toehold of probe B to complete the CHA, generating the partial duplex B/C. Furthermore, toeholds of the B/C duplex can assemble a DNAzyme-cascaded hydrolysis reaction, cleaving the substrate strand DNA2, resulting in the high fluorescence signal. Meanwhile, the assembly process of the AND−INHIBIT logic gate was further confirmed by PAGE results (Figure S8, Supporting Information). The output of this logic operation is depicted in Figure 3B. The truth table is presented in Figure 3C. The input combinations of 0/0/0, 0/1/0, 0/0/1, 0/1/1, 1/0/0, 1/0/1, and 1/1/1 generate an output of 0, and the input combination of 1/1/0 generates an output of 1. We used the AND−INHIBIT logic gate to test the white wine samples spiked with the tree inputs, and the results are shown in Figure S9 (Supporting Information).

Using the same three inputs and different recognition probes, we also constructed an INHIBIT−OR connected logic

https://doi.org/10.1021/acs.analchem.1c05485
Anal. Chem. 2022, 94, 3693−3700

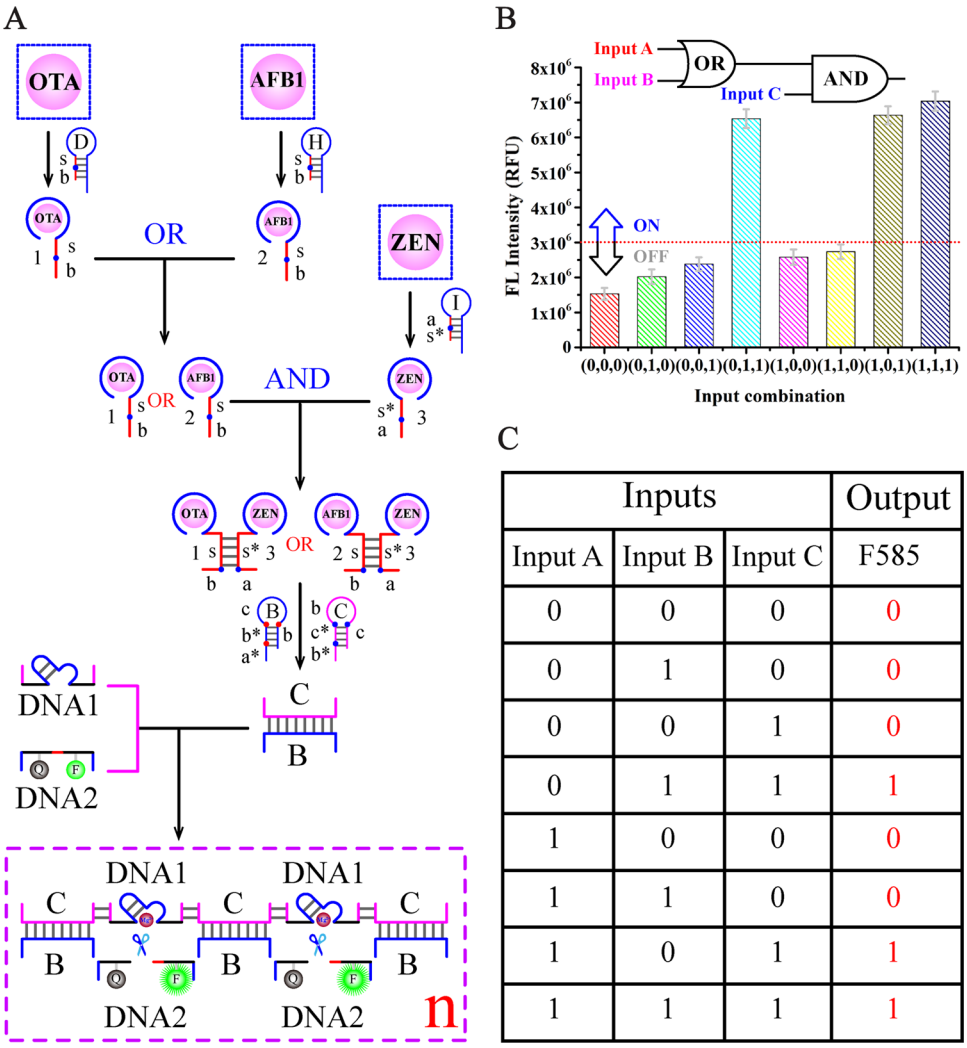

C

Inputs			Output
Input A	Input B	Input C	F585
0	0	0	0
0	1	0	0
0	0	1	0
0	1	1	1
1	0	0	0
1	1	0	0
1	0	1	1
1	1	1	1

Figure 5. (A) Schematic illustration of the OR−AND logic gate. (B) Histogram presentation of the corresponding fluorescence intensities at 585 nm. The red dashed line shows the threshold value of 3.0 × 10^6. (C) Truth table of the OR−AND logic gate.

gate (Figure 4A). In the presence of input A, the binding between probe A and OTA will release the trigger DNA 1 (domains a and b). In the same way, the trigger DNA 2 (domains b* and a*) will also be released when probe G recognizes and binds to input B (AFB1). The trigger DNAs 1 and 2 are complementary nucleic acids. If the trigger DNA 2 (domains b* and a*) is free in the sensing system, it will inhibit the trigger DNA 1 (domains a and b) from initiating the subsequent logic operation. In the presence of input C, another trigger DNA 3 (domains a and b) in probe S will be released into the sensing system, which possesses the same sequence as DNA 1. As a result, either the trigger DNA 1 or 3 can activate the hairpin assembly, yielding a high fluorescence signal. Meanwhile, the assembly process of the INHIBIT−OR logic gate was further confirmed by PAGE results (Figure S10, Supporting Information). The output of this logic operation is depicted in Figure 4B. The truth table is presented in Figure 4C. The input combinations of 0/0/0, 0/1/0, 0/1/1, and 1/1/0 generate an output of 0, and the input combinations of 0/0/1, 1/0/0, 1/0/1, and 1/1/1 generate an output of 1.

Furthermore, we designed an OR−AND connected logic gate using the same inputs (Figure 5A). In the presence of input A, the binding between probe D and OTA will release the trigger DNA 1 (domains s and b). In the same way, the trigger DNA 2 (domains s and b) will also be released when probe H recognizes and binds to input B. The trigger DNAs 1 and 2 have the same nucleic acids. In the presence of input C, the trigger DNA 3 (domains a and s*) in probe I will be liberated, which possesses a partially complementary sequence with the trigger DNA 1 or 2. As a result, the trigger DNA 3 (domains a and s*) will hybridize with the trigger DNA 1 or 2 to form a partial duplex complex (1−3) or (2−3). The formed duplex complex will initiate the toehold-mediated cascade catalytic assembly, resulting in a high fluorescence signal. Meanwhile, the assembly process of the OR−AND connected logic gate was further confirmed by PAGE results (Figure S11, Supporting Information). The output of this logic operation is depicted in Figure 5B. The truth table is presented in Figure 5C. The input combinations of 0/0/0, 1/0/0, 0/1/0, 1/1/0, and 0/0/1 generate an output of 0, and the input combinations of 1/0/1, 0/1/1, and 1/1/1 generate an output of 1.

Finally, we designed an OR−INHIBIT connected logic gate (Figure S12A, Supporting Information). In the presence of input A, the binding between probe A and OTA will release the trigger DNA 1 (domains a and b). In the same way, the trigger DNA 2 (domains a and b) will also be released when probe S recognizes and binds to input B (AFB1). The trigger DNAs 1 and 2 are the same nucleic acids. In the presence of

https://doi.org/10.1021/acs.analchem.1c05485
Anal. Chem. 2022, 94, 3693−3700

input C, probe J will liberate the caged trigger DNA 3 (domains b* and a*), which possesses the complementary sequence with the trigger DNAs 1 and 2. If the trigger DNA 3 is liberated in the logic system, it will prevent the trigger DNAs 1 and 2 from launching the toehold-mediated cascade catalytic assembly. Thus, the trigger DNAs 1 and 2 can initiate the toehold-mediated cascade catalytic assembly, resulting in a high fluorescence signal. Meanwhile, the assembly process of the OR−INHIBIT logic gate was further confirmed by PAGE results (Figure S13, Supporting Information). The output of this logic operation is depicted in Figure S12B. The truth table is presented in Figure S12C. The input combinations of 0/0/0, 1/0/1, 0/1/1, 1/1/1, and 0/0/1 generate an output of 0, and the input combinations of 1/0/0, 0/1/0, and 1/1/0 generate an output of 1.

CONCLUSIONS

In summary, an enzyme-free toehold-mediated cascade catalytic assembly has been designed for a mycotoxin assay based on the CHA and DNAzyme-cascaded hydrolysis reaction. This sensing platform was sensitive, enabling the fluorescence detection of OTA as low as 0.2 pM. By changing the aptamer sequence, the biosensing was further extended for the detection of AFB1 and ZEN with LODs of 0.13 and 0.17 pM, respectively. The mycotoxin system was robust and was applied for the quantitative analysis of OTA, AFB1, and ZEN in wine samples with excellent selectivity and good reliability. Due to the advantages of flexibility and versatility, this biosensing platform was used to fabricate several concatenated logic gates, including AND−INHIBIT, INHIBIT−OR, OR−AND, and OR−INHIBIT logic operations. OTA, AFB1, and ZEN were set as input A, input B, and input C, respectively. The inputs were coded as 1 when they were present and 0 when they were absent. In the AND−INHIBIT logic gate, the 1/1/0 input combination generates an output of 1. In the INHIBIT−OR logic gate, the input combinations of 0/0/1, 1/0/0, 1/0/1, and 1/1/1 generate an output of 1. In the OR−AND logic gate, the input combinations of 1/0/1, 0/1/1, and 1/1/1 generate an output of 1. In the OR−INHIBIT logic gate, the input combinations of 1/0/0, 0/1/0, and 1/1/0 generate an output of 1. Such multiple functions of the logic system provided a universal sensing strategy for the intelligent detection of multiple mycotoxins.

ASSOCIATED CONTENT

Supporting Information

The Supporting Information is available free of charge at https://pubs.acs.org/doi/10.1021/acs.analchem.1c05485.

DNA sequences (Tables S1−S5); PAGE confirmation of the formation of ($[B/C/DNA1/DNA2]_n$) (Figure S1); optimization of experimental conditions (Figures S2−S5); analytical performance for AFB1 with different concentrations (Figure S6); analytical performance for ZEN with different concentrations (Figure S7); PAGE analysis of the assembly process of the logic gates (Figures S8, S10, S11, and S13); real sample assay using the AND−INHIBIT logic gate (Figure S9); schematic illustration of the OR−INHIBIT logic gate (Figure S12); detection sensitivity comparison (Table S6); real sample analysis (Table S7); and logic sensitivity comparison (Table S8) (PDF)

AUTHOR INFORMATION

Corresponding Author

Junhua Chen − *National-Regional Joint Engineering Research Center for Soil Pollution Control and Remediation in South China, Guangdong Key Laboratory of Integrated Agro-environmental Pollution Control and Management, Institute of Eco-environmental and Soil Sciences, Guangdong Academy of Sciences, Guangzhou 510650, China;* orcid.org/0000-0001-9450-7272; Email: 222chenjunhua@163.com, jhchen@soil.gd.cn

Authors

Jiafeng Pan − *College of Bioscience and Biotechnology, Hunan Agricultural University, Changsha 410128, China; National-Regional Joint Engineering Research Center for Soil Pollution Control and Remediation in South China, Guangdong Key Laboratory of Integrated Agro-environmental Pollution Control and Management, Institute of Eco-environmental and Soil Sciences, Guangdong Academy of Sciences, Guangzhou 510650, China*

Fang Deng − *College of Bioscience and Biotechnology, Hunan Agricultural University, Changsha 410128, China; National-Regional Joint Engineering Research Center for Soil Pollution Control and Remediation in South China, Guangdong Key Laboratory of Integrated Agro-environmental Pollution Control and Management, Institute of Eco-environmental and Soil Sciences, Guangdong Academy of Sciences, Guangzhou 510650, China*

Zhi Liu − *College of Bioscience and Biotechnology, Hunan Agricultural University, Changsha 410128, China*

Gu Shi − *National-Regional Joint Engineering Research Center for Soil Pollution Control and Remediation in South China, Guangdong Key Laboratory of Integrated Agro-environmental Pollution Control and Management, Institute of Eco-environmental and Soil Sciences, Guangdong Academy of Sciences, Guangzhou 510650, China*

Complete contact information is available at: https://pubs.acs.org/10.1021/acs.analchem.1c05485

Notes

The authors declare no competing financial interest.

ACKNOWLEDGMENTS

This work was supported by the Guangdong Basic and Applied Basic Research Foundation (2021A1515012192), the Provincial Excellent Doctoral Dissertation Cultivation Fund of Hunan Agricultural University (YB2019001), and the Graduate Student Research Innovation Project of Hunan Province (CX20200654).

REFERENCES

(1) Rivas, L.; Mayorga-Martinez, C. C.; Quesada-Gonzalez, D.; Zamora-Galvez, A.; de la Escosura-Muniz, A.; Merkoci, A. *Anal. Chem.* **2015**, *87*, 5167−5172.

(2) Feng, J.; Li, Y.; Gao, Z.; Lv, H.; Zhang, X.; Fan, D.; Wei, Q. *Biosens. Bioelectron.* **2018**, *99*, 14−20.

(3) Viter, R.; Savchuk, M.; Iatsunskyi, I.; Pietralik, Z.; Starodub, N.; Shpyrka, N.; Ramanaviciene, A.; Ramanavicius, A. *Biosens. Bioelectron.* **2018**, *99*, 237−243.

(4) Xing, K.; Peng, J.; Shan, S.; Liu, D.; Huang, Y.; Lai, W. *Anal. Chem.* **2020**, *92*, 8422−8426.

(5) Giovannoli, C.; Passini, C.; Di Nardo, F.; et al. *J. Agric. Food Chem.* **2014**, *62*, 5220−5225.

(6) Olsson, J.; Börjesson, T.; Lundstedt, T.; Schnürer, J. *Int. J. Food Microbiol.* **2002**, *72*, 203−214.
(7) Campone, L.; Piccinelli, A. L.; Celano, R.; Pagano, I.; Russo, M.; Rastrelli, L. *Food Chem.* **2018**, *244*, 128−135.
(8) Zhang, K.; Zhang, J.; Wang, F.; Kong, D. *ACS Sens.* **2021**, *6*, 2261−2269.
(9) Tian, F.; Zhou, J.; Jiao, B.; He, Y. *Nanoscale* **2019**, *11*, 9547−9555.
(10) Zhang, X.; Zhi, H.; Zhu, M.; Wang, F.; Meng, H.; Feng, L. *Biosens. Bioelectron.* **2021**, *180*, No. 113146.
(11) Wang, S.; Zhang, Y.; Pang, G.; Zhang, Y.; Guo, S. *Anal. Chem.* **2017**, *89*, 1704−1709.
(12) Wang, Z.; Yu, H.; Han, J.; Xie, G.; Chen, S. *Chem. Commun.* **2017**, *53*, 9926−9929.
(13) Zhu, C.; Liu, D.; Li, Y.; Ma, S.; Wang, M.; You, T. *Biosens. Bioelectron.* **2021**, *174*, No. 112654.
(14) Zheng, F.; Ke, W.; Shi, L.; Liu, H.; Zhao, Y. *Anal. Chem.* **2019**, *91*, 11812−11820.
(15) Huang, X.; Wu, S.; Hu, H.; Sun, J. *ACS Sens.* **2020**, *5*, 2636−2643.
(16) Zhang, S.; Luan, Y.; Xiong, M.; Zhang, J.; Lake, R.; Lu, Y. *ACS Appl. Mater. Interfaces* **2021**, *13*, 9472−9481.
(17) Maram, R.; van Howe, J.; Kong, D.; Ros, F. D.; Guan, P.; Galili, M.; Morandotti, R.; Oxenløwe, L. K.; Azaña, J. *Nat. Commun.* **2020**, *11*, No. 5839.
(18) Miao, P.; Tang, Y. *ACS Cent. Sci.* **2021**, *7*, 1036−1044.
(19) Yu, Y.; Guo, Q.; Jiang, W.; Zhang, H.; Cai, C. *Anal. Chem.* **2021**, *93*, 11298−11304.
(20) Xiao, M.; Zhou, Q.; Zhang, H.; Zhou, L.; Ma, J.; Yi, C. *ACS Appl. Nano Mater.* **2021**, *4*, 8184−8191.
(21) Zheng, J.; Wang, Q.; Shi, L.; Peng, P.; Shi, L.; Li, T. *Angew. Chem., Int. Ed.* **2021**, *60*, 20858−20864.
(22) Kim, K. T.; Angerani, S.; Winssinger, N. *Chem. Sci.* **2021**, *12*, 8218−8223.
(23) Pan, J.; He, Y.; Liu, Z.; Chen, J. *Chem. Commun.* **2021**, *57*, 1125−1128.
(24) Fan, D.; Wang, E.; Dong, S. *Chem. Sci.* **2017**, *8*, 1888−1895.
(25) Du, J.; Wang, J.; Huang, W.; Deng, Y.; He, Y. *Anal. Chem.* **2018**, *90*, 9959−9965.
(26) Tregubov, A. A.; Nikitin, P. I.; Nikitin, M. P. *Chem. Rev.* **2018**, *118*, 10294−10384.
(27) Fernandez, A.; Thompson, E. J.; Pollard, J. W.; Kitamura, T.; Vendrell, M. *Angew. Chem., Int. Ed.* **2019**, *58*, 16894−16898.
(28) Feng, D.; Liu, G. *Anal. Chem.* **2021**, *93*, 8326−8335.
(29) Jia, H.; Zhu, Y.; Duan, Q.; Wu, F. *Chem. Soc. Rev.* **2021**, *50*, 6240−6277.
(30) Yang, Y.; Xu, J.; Sun, Y.; Mo, L.; Liu, B.; Pan, X.; Liu, Z.; Tan, W. *J. Am. Chem. Soc.* **2021**, *143*, 8391−8401.
(31) Melkonian, A. V.; Loppinet, E.; Martin, R.; Porteus, M.; Khosla, C. *J. Am. Chem. Soc.* **2021**, *143*, 10537−10540.
(32) Ho, T. Y. H.; Shao, A.; Lu, Z.; Savilahti, H.; Menolascina, F.; Wang, L.; Dalchau, N.; Wang, B. *Nat. Commun.* **2021**, *12*, No. 2200.
(33) Yu, Y.; Guo, Q.; Jiang, W.; Zhang, H.; Zhang, C. *Anal. Chem.* **2021**, *93*, 11298−11304.
(34) Zhu, L.; Yu, L.; Yang, X. *ACS Appl. Mater. Interfaces* **2021**, *13*, 42250−42257.
(35) Wang, J.; Li, Z.; Zhou, Z.; Ouyang, Y.; Zhang, J.; Ma, X.; Tian, H.; Willner, I. *Chem. Sci.* **2021**, *12*, 11204−11212.
(36) Liu, X.; Meng, F.; Sun, R.; Wang, K.; Yu, Z.; Miao, P. *Chem. Commun.* **2021**, *57*, 2629−2632.
(37) Pan, J.; He, Y.; Liu, Z.; Chen, J. *Anal. Chem.* **2022**, *94*, 714−722.
(38) Turkoglu, G.; Koygun, G. K.; Yurt, M. N. Z.; Pirencioglu, S. N.; Erbas-Cakmak, S. *Chem. Sci.* **2021**, *12*, 9754−9758.
(39) Zhang, Y.; Wang, F.; Chao, J.; Xie, M.; Liu, H.; Pan, M.; Kopperger, E.; Liu, X.; Li, Q.; Shi, J.; Wang, L.; Hu, J.; Wang, L.; Simmel, F. C.; Fan, C. *Nat. Commun.* **2019**, *10*, No. 5469.
(40) Lustgarten, O.; Carmieli, R.; Motiei, L.; Margulies, D. *Angew. Chem., Int. Ed.* **2019**, *58*, 184−188.
(41) Lv, W.; Li, C.; Li, Y.; Zhen, S.; Huang, C. *Anal. Chem.* **2021**, *93*, 3411−3417.
(42) Lv, M.; Zhou, W.; Fan, D.; Guo, Y.; Zhu, X.; Ren, J.; Wang, E. *Adv. Mater.* **2020**, *32*, No. 1908480.
(43) Chen, J.; Chen, S.; Li, F. *Anal. Chem.* **2018**, *90*, 10311−10317.
(44) Zhou, Z.; Wang, J.; Levine, R. D.; Remacle, F.; Willner, I. *Chem. Sci.* **2021**, *12*, 5473−5483.
(45) Mi, Y.; Zhao, J.; Chu, H.; Li, Z.; Yu, M.; Li, L. *Anal. Chem.* **2021**, *93*, 2500−2509.

https://doi.org/10.1021/acs.analchem.1c05485
Anal. Chem. 2022, 94, 3693−3700